Structural Durability & Health Monitoring

Tech Science Press

https://doi.org/10.32604/sdhm.2026.081450

ARTICLE

Mechanisms of Differential Settlement in Widened Embankments over Soft Soil Considering Structural Degradation and Geometric Coupling: Physics-Constrained Intelligent Prediction

Hongxing Li[1], **Xizhong Xu**[2,*], **Liang Wang**[1], **Jiabo Hu**[2] **and Zhice Zhao**[1]

[1]Cangzhou Transportation Development (Group) Co., Ltd., Cangzhou, China
[2]Shandong Transportation Research Institute, Jinan, China

*Corresponding Author: Xizhong Xu. Email: xxuu125896321@163.com

Received: 02 March 2026; Accepted: 08 April 2026; Published: 24 August 2026

ABSTRACT: Differential settlement control in highway widening projects on soft soil remains a major challenge. This study investigates the mechanisms of differential settlement in widened embankments and develops an intelligent prediction framework by integrating high-fidelity numerical simulations with physics-constrained deep learning. First, comprehensive numerical simulations were performed using a Hardening Soil (HS) model considering structural degradation in PLAXIS 2D. This work revealed the redistribution of additional stress under widening loads and elucidated the evolution mechanisms of plastic zone development and interface shear behavior at the junction of new and existing subgrades. A reasonable step width range of 1.5–2.0 m is identified based on deformation control, plastic zone extent, and engineering economy. To overcome the limited physical consistency of conventional deep learning, a physics-constrained WOA-Attention-BiGRU framework is developed by embedding monotonicity and logarithmic consolidation rate decay as regularization terms in the loss function, significantly improving robustness and interpretability in data-sparse regimes. Validation shows R^2 = 0.988 and RMSE ≤ 3.2 mm for full-time-series settlement prediction, substantially outperforming pure data-driven models; slight error increase occurs under extreme soft conditions but remains within engineering tolerances. The findings elucidate the nonlinear coupling mechanisms between geometric parameters and foundation stiffness governing differential settlement gradients, providing reliable support for optimized design and long-term settlement assessment in soft soil highway widening projects.

KEYWORDS: Highway widening; differential settlement; structured soft soil; physics-constrained deep learning; Attention mechanism; geometric optimization

1 Introduction

Against the backdrop of the rapid development of modern transportation infrastructure, the contradiction between the capacity of existing highways and the continuously growing traffic demand has become increasingly prominent. To alleviate traffic bottlenecks and enhance the overall efficiency of the road network, highway widening has become a crucial direction in global transportation planning. However, controlling the coordinated deformation between new and existing subgrades during the widening process remains a core challenge in geotechnical engineering. Due to significant differences in loading history, consolidation degree, and soil microstructure, the new and existing subgrades exhibit highly asymmetric mechanical responses under the additional widening loads [1]. If differential settlement is not effectively identified and regulated, it can induce longitudinal pavement cracks, shear failure at the splicing interface, and overall subgrade instability, severely impacting the service life and operational safety of the road. Therefore, systematically revealing the mechanisms of differential settlement in widened embankments and establishing a high-precision prediction model has become a critical scientific problem to be solved for highway widening projects in soft soil regions [2].

The mechanical behavior of soft soil foundations is deeply influenced by their natural structural characteristics. As a typical highly structured material, soft soil exhibits complex nonlinear degradation features in shear strength and compressive modulus under construction disturbance and asymmetric incremental loading. Traditional geotechnical constitutive models are mostly based on the assumption of remolded soil, making it difficult to accurately describe the stress redistribution and damage accumulation during the structural degradation of natural soil. In recent years, researchers have quantitatively characterized the structural damage evolution during the consolidation-shear coupling process by introducing structural parameters to modify advanced constitutive models, such as the Hardening Soil model [3]. This approach provides a more reliable theoretical basis for analyzing the stress concentration and local failure mechanisms at the junction of new and old subgrades, holding significant importance for mitigating engineering risks caused by structural soil failure.

From the perspective of structural design, the geometric optimization of the splicing interface is an effective way to mitigate differential deformation. Step excavation, as a key technique connecting new and existing subgrades, directly affects mechanical interlocking and shear stress transfer efficiency. Reasonably increasing the step width can expand the shear deformation band and reduce the local settlement gradient, but its potential impact on the stability of existing slopes must also be considered [4]. Meanwhile, the embankment aspect ratio, as a key parameter controlling the overall geometric morphology, significantly regulates the distribution of additional stress in the foundation. Under small aspect ratios, stress superposition is exacerbated, easily forming distinct settlement troughs at the slope toe and increasing differential settlement [5]. Although engineering practices have accumulated considerable experience, systematic parameter sensitivity analyses addressing multi-parameter coupling and varying foundation strengths remain insufficient, necessitating refined geometric optimization studies.

Numerical simulation (Finite Element Method) has become an important tool for analyzing complex foundation responses [6]. However, for rapid assessment under repeated working conditions and timely interpretation of field monitoring data, conventional finite element simulation alone may be computationally expensive; therefore, settlement prediction methods and simplified surrogate strategies are needed as effective complements [7]. The introduction of artificial intelligence methods provides an effective supplement. The Bidirectional Gated Recurrent Unit (BiGRU) demonstrates excellent adaptability in handling the hysteresis and non-stationary characteristics of consolidation settlement time-series data [8]; the Attention mechanism can further enhance the model's ability to dynamically allocate weights to key physical variables [9]. Nevertheless, purely data-driven models often lack physical interpretability and easily violate basic physical laws, such as the monotonic increase and rate decay of the consolidation process. Therefore, embedding prior physical laws into the loss function to construct a physics-constrained deep learning model has become a frontier approach to improving the robustness and mechanical consistency of geotechnical prediction models [10–12].

Metaheuristic optimization methods, such as the Whale Optimization Algorithm (WOA), demonstrate strong global search capabilities in optimizing deep learning hyperparameters [13]. By integrating WOA, the Attention mechanism, and BiGRU, and applying physical constraints, a surrogate model combining mechanical depth and computational efficiency can be constructed. This model can rapidly respond to settlement prediction needs under different combinations of foundation modulus, step width, and aspect ratio, thereby providing efficient support for settlement evaluation, design optimization, and dynamic construction control [14–16]. The research paradigm combining mechanism analysis and intelligent prediction holds significant theoretical and practical value for advancing the intelligent construction of transportation infrastructure.

Targeting the differential settlement control in highway widening, this study conducts systematic research across three aspects: structural constitutive response, geometric parameter influence, and physics-constrained intelligent prediction. First, based on the HS model considering structural degradation, numerical simulations are performed to reveal the stability evolution of the junction under varying foundation strengths. Second, the impacts of step width and embankment aspect ratio on the spatial distribution of differential settlement are quantitatively analyzed to determine the optimal geometric parameter range. Finally, a physics-constrained WOA-Attention-BiGRU prediction framework is constructed to achieve high-precision simulation and early warning of full-lifecycle embankment settlement, providing theoretical support and technical references for widening designs in soft soil areas.

2 Construction of Numerical Platform and Analysis of Widening Mechanisms

2.1 Selection of Geotechnical Constitutive Model Considering Structural Degradation

Accurate simulation of the mechanical response of soft soil foundations is a prerequisite for differential settlement analysis. Naturally deposited soft soils usually possess apparent initial structure, with shear strength and compressibility controlled by particle cementation and microscopic pore structures.

Under widening loads, the soil structure undergoes irreversible degradation, directly affecting the overall stability of the splicing interface [17,18]. Given the significant shear softening and compression hardening behaviors of soft soil under asymmetric incremental loads, the Hardening Soil (HS) model is selected as the basic constitutive framework in this study. Unlike traditional models that rely on a single generic compression modulus, the HS model accurately captures the stress-dependent nonlinear stiffness evolution by distinguishing three distinct moduli: the secant modulus from standard drained triaxial tests ($E_{\_50}$), which controls the magnitude of shear deformation prior to failure; the tangent stiffness for primary oedometer loading ($E_{\_oed}$), which governs one-dimensional compression and consolidation settlement; and the unloading/reloading modulus ($E_{\_ur}$), which dictates the elastic reversible deformation during excavation or cyclic loading. The specific geotechnical parameters employed in this study are detailed in Table 1.

Table 1: Geotechnical parameters used in numerical simulations.

Material Type	Model	γ (kN/m^3)	$E_{\_50}$ (MPa)	$E_{\_oed}$ (MPa)	$E_{\_ur}$ (MPa)	C' (kPa)	φ' (°)	k (m/d)
Embankment Fill	HS	20.0	45.0	45.0	135.0	1.0	35.0	–
Soft Clay 1	HS	17.5	3.2	3.2	10.5	8.0	22.0	1.0e−4
Soft Clay 2	HS	17.8	5.0	4.8	15.0	12.0	24.0	8.0e−4
Stiff Clay	HS	18.5	15.0	14.0	45.0	25.0	28.0	5.0e−4

Table 1 summarizes the main geotechnical physical and mechanical parameters adopted in the numerical simulations. These parameter values were comprehensively determined based on laboratory triaxial tests, oedometer tests, and field monitoring data from typical soft soil regions. Specifically, the stiffness parameters ($E_{\_50}$, $E_{\_oed}$, and $E_{\_ur}$) and the permeability coefficients (k) of the soft clay layers (Soft Clay 1 and Soft Clay 2) accurately reflect the distinct structural and drainage characteristics resulting from varying depositional environments. The parameters assigned to the stiff clay layer simulate the rigid restraining effect of the underlying bearing stratum on deep settlement, while the embankment fill properties are strictly based on conventional compaction standards.

To quantitatively describe the structural degradation process, a damage factor related to cumulative plastic shear strain is introduced to characterize the progressive softening of effective cohesion and internal friction angle:

$$c'\left(\varepsilon_s^p\right) = c'_0 \cdot \left[1 - \alpha_c \cdot \tanh\left(\beta_c \cdot \varepsilon_s^p\right)\right] \tag{1}$$

$$\varphi'\left(\varepsilon_s^p\right) = \varphi'_0 \cdot \left[1 - \alpha_\varphi \cdot \tanh\left(\beta_\varphi \cdot \varepsilon_s^p\right)\right] \tag{2}$$

In Eqs. (1) and (2), $c'(\epsilon_s^p)$ and $\varphi'(\epsilon_s^p)$ denote the effective cohesion and effective internal friction angle at a given plastic shear strain ϵ_s^p, respectively. The terms $c_0^{'}$ and $\varphi_0^{'}$ represent the initial strength parameters of the soil. The coefficients α and β signify the damage evolution parameters that govern the magnitude and the rate of structural strength degradation, respectively. The rationale for choosing the hyperbolic tangent (tanh) function lies in its ability to smoothly and continuously capture the progressive transition from an initial intact structured state to a fully destructured (remolded) state. Previous studies have also demonstrated the applicability of HS/HSS-type constitutive models in deformation analyses of soft soils when stress-dependent stiffness and structural effects are properly considered [19,20]. Specifically, the calibration of these parameters was conducted through laboratory isotropically consolidated undrained (CU) triaxial tests: parameter α is determined by the difference between the peak and residual strengths, while parameter β is derived by fitting the slope of the post-peak stress-strain softening curve. This model captures both pre-peak stiffness hardening and post-peak strength softening. The structural degradation pattern of the soil is shown in Fig. 1. As the stress-strain evolution curve demonstrates, the soil exhibits high initial tangent stiffness primarily provided by cementation resistance. As deviatoric stress increases, the structural yield point is breached, leading to irreversible skeletal damage and significant strain-softening, eventually reaching a residual strength state. This macroscopic reproduction of microscopic structural degradation provides vital constitutive support for accurately capturing local shear failure at the splicing interface.

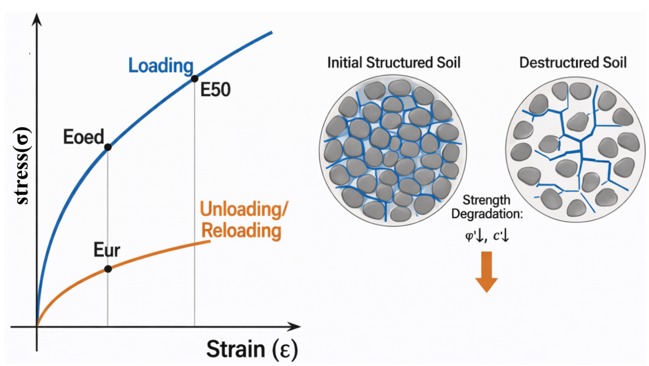

Figure 1: Mechanical characteristics of HS model and structural degradation.

2.2 Numerical Simulation Scheme and Boundary Conditions

PLAXIS 2D software is employed to establish a typical single-sided highway widening cross-section model. The total transverse width is set to 120 m, and the vertical depth is 40 m. According to standard geotechnical numerical modeling practices, the lateral boundaries are positioned at a distance of more than three to five times the embankment base width from the slope toe. Furthermore, the bottom boundary extends deep into the stiff underlying stratum, where the additional vertical stress increment induced by the widening load decays to less than 5% of the applied surface stress. This rigorous spatial configuration sufficiently eliminates boundary effects on the deep stress distribution. The long-term service state of the existing subgrade is simulated through a coupled consolidation analysis in PLAXIS. Before initiating the widening phases, a preliminary consolidation stage is conducted under the original embankment loading until the excess pore water pressure dissipates to a point where the degree of consolidation exceeds 95%. This ensures that the stress history and skeletal hardening of the foundation under long-term service are realistically captured. Regarding the constitutive framework, although the Modified Cam-Clay (MCC) model is a conventional choice for consolidation, the Hardening Soil (HS) model was deliberately selected for its superior ability to handle complex asymmetric loading paths. Unlike the MCC model, the HS model accounts for stress-dependent stiffness and differentiates between the shear modulus (E_{50}), oedometer modulus ($\boldsymbol{E_{oed}}$), and unloading/reloading modulus (E_{ur}), providing significantly higher precision in capturing the nonlinear stiffness evolution and shear-induced deformations characteristic of highway widening on soft soil. The widened side involves fill heights varying from 4 to 10 m to adjust the embankment aspect ratio. The calculation strictly follows the actual construction sequence: surface clearing of the existing slope, step excavation, geogrid laying, and layered filling. The shear performance of the contact surface is characterized by the interface strength reduction factor Rinter.

The detailed geometric dimensions, finite element mesh, and boundary conditions for the embankment widening model are illustrated in Fig. 2. Local mesh refinement is applied at the existing slope, splicing steps, and underlying soft soil layers to balance computational efficiency and local deformation accuracy. Displacement boundaries are fixed at the base and normally constrained on the sides; hydraulic boundaries are permeable at the surface and impermeable at the bottom and sides, strictly adhering to realistic hydrogeological conditions. To accurately reflect the hydrological environment characteristic of typical soft soil regions, the groundwater table is positioned at a depth of 1.0 m below the natural ground surface. This condition is implemented in the PLAXIS numerical framework by defining a phreatic level, which establishes the initial hydrostatic pore water pressure distribution. Throughout the coupled consolidation phases, the evolution of effective stress is strictly governed by the generation and dissipation of excess pore water pressure. The hydraulic response is dictated by the permeability coefficients (k) specified in Table 1. This configuration ensures that the numerical model precisely captures the dynamic evolution of pore water pressure under asymmetric widening loads.

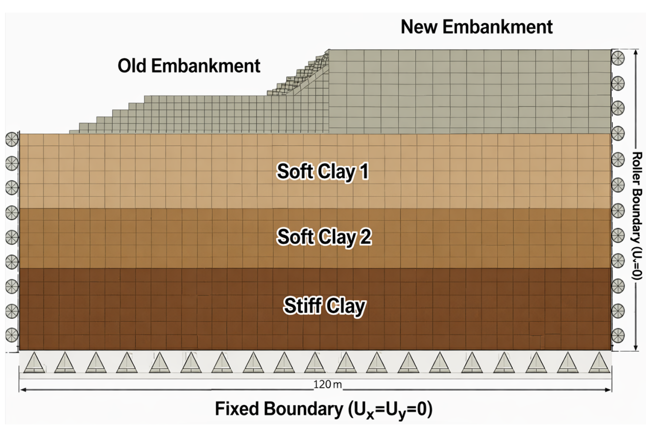

Figure 2: Geometric dimensions, finite element mesh, and boundary conditions for embankment widening.

It is worth noting that highway widening is inherently a three-dimensional (3D) spatial problem. However, since highway embankments are typical linear structures where the longitudinal length is significantly greater than the transverse width, the deformation along the longitudinal direction is strictly constrained.

Therefore, applying the 2D plane strain assumption is a reasonable and widely accepted standard approach for evaluating cross-sectional settlement in geotechnical engineering. Furthermore, generating the 1200 large-scale finite element samples required to train the deep learning model necessitates balancing computational efficiency with mechanical accuracy, an objective that the 2D model achieves effectively. Nevertheless, the 2D analysis has certain limitations compared to 3D simulations. Specifically, it cannot capture 3D spatial effects such as longitudinal stiffness variations, uneven construction staging along the roadway, and the spatial variability of soft soil properties. These 3D features may induce localized longitudinal differential settlement, which will be the primary focus of our future expanded 3D numerical and intelligent prediction studies.

2.3 Geometric Effects of Step Excavation and Spatial Deformation Patterns

Step excavation is critical for enhancing the coordinated deformation capacity of new and existing subgrades. By adjusting the step width, the stress transfer path at the interface is significantly optimized [21]. Results show that as the step width increases, the strain concentration at the junction notably decreases, and shear stresses gradually propagate laterally into the steps, effectively reducing relative differential settlement.

Fig. 3 illustrates the mechanical response of the foundation under step widths of 1.0 and 2.5 m. The color contours represent the magnitude of equivalent stress and strain increments, where red indicates high-value regions and blue indicates low-value regions. The plastic zone (Fig. 3c) is defined based on the Mohr-Coulomb failure criterion; specifically, a region is identified as a plastic zone when the stress state of the soil elements reaches the strength envelope. Quantitative analysis of the plastic zones and shear strain increments (Fig. 3c,d) demonstrates that increasing the step width from 1.0 to 2.5 m reduces the cumulative plastic zone area by approximately 41% and significantly lowers peak shear strain. This indicates that wider steps mitigate plastic zones and promote uniform shear band expansion, reducing shear failure risks.

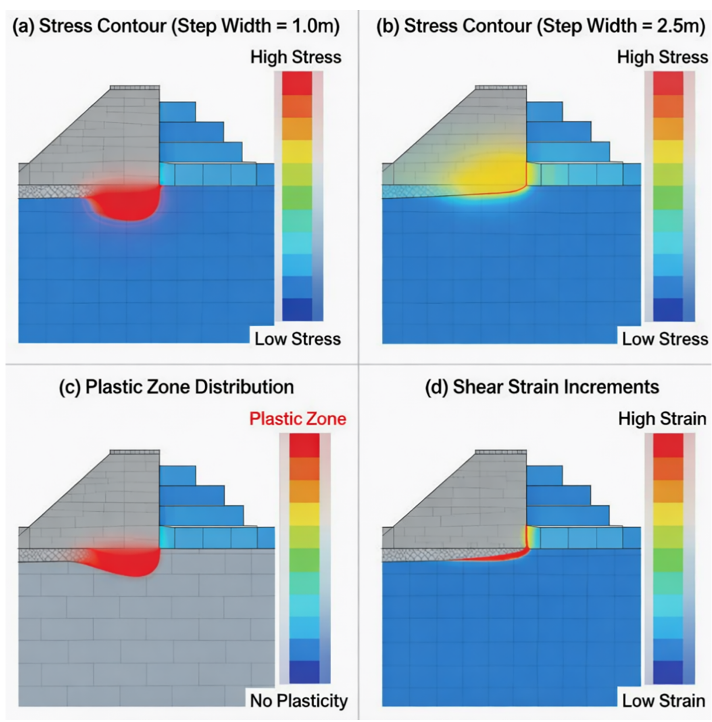

Figure 3: Mechanical response under step excavation: (**a**) 1.0 m step stress contour; (**b**) 2.5 m step stress contour; (**c**) Plastic zone distribution; (**d**) Shear strain increments.

2.4 Influence of Embankment Aspect Ratio on Additional Stress Field

The embankment aspect ratio is a core geometric parameter governing additional stress distribution. Simulations show that embankment geometry significantly alters internal stress trajectories [22]. Increasing the aspect ratio expands the "stress shadow", promoting uniform deep stress diffusion and reducing interface settlement gradients [23]. Fig. 4a shows that under a small aspect ratio (high fill, narrow base), localized loading creates deep, narrow stress bulbs, causing severe stress decay at the slope toe, risking lateral extrusion. Conversely, a large aspect ratio (Fig. 4b) yields flatter, wider stress contours, significantly lowering stress increments per unit depth. The transverse settlement profiles in Fig. 4c reflect this: small aspect ratios induce steep settlement gradients, while large ratios produce smooth transitions, homogenizing the differences.

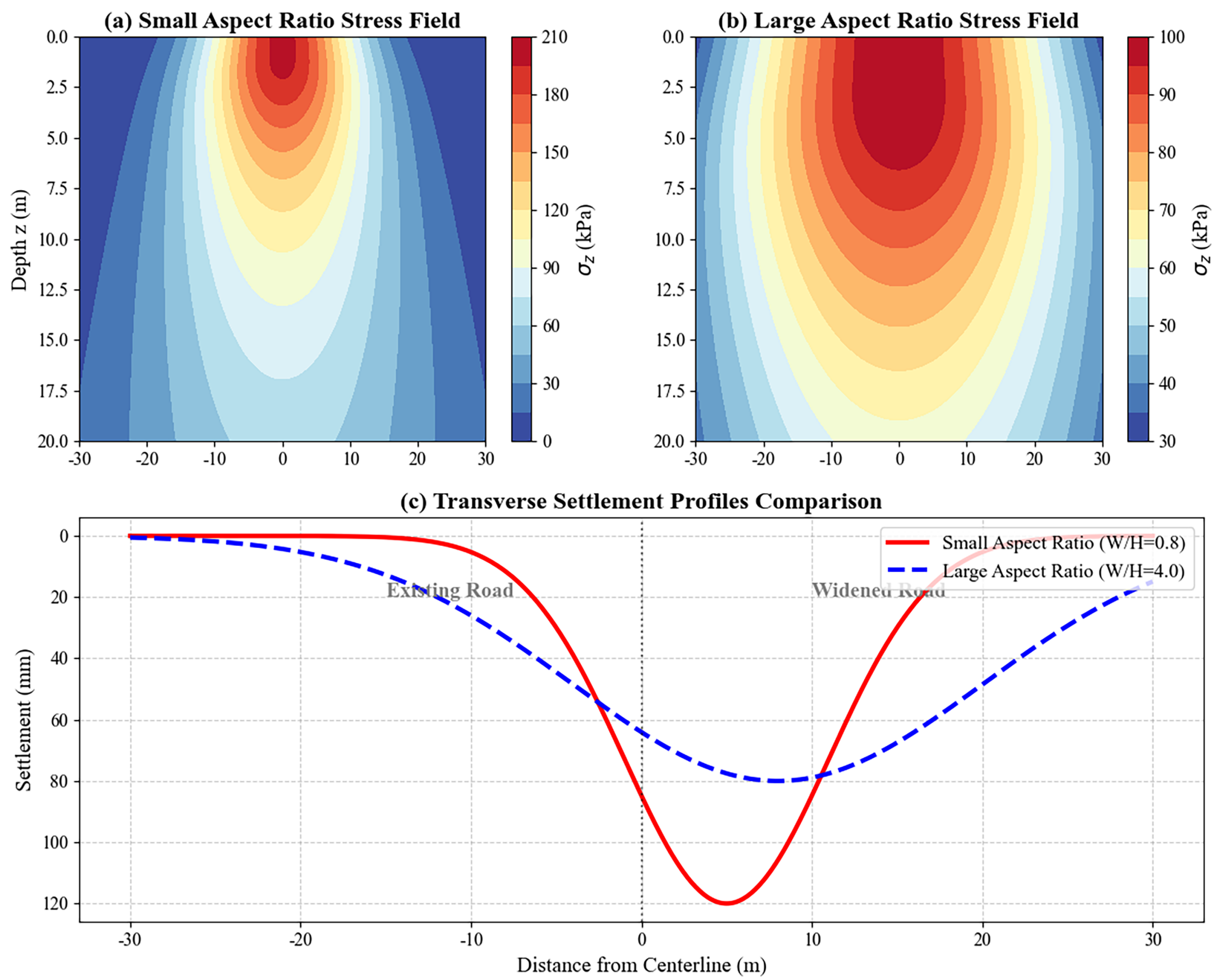

Figure 4: Foundation stress and deformation under different aspect ratios: (**a**) Small aspect ratio stress field; (**b**) Large aspect ratio stress field; (**c**) Transverse settlement profiles.

Fig. 5 illustrates the time-evolution curves of settlement at key monitoring points. The new side exhibits rapid early settlement driven by instantaneous compression and pore pressure dissipation. During the transitional phase (100–300 days post-construction), the rate undergoes logarithmic decay. In the long-term phase, cumulative settlement stabilizes via secondary creep. The vertical gap between the curves represents the crucial differential settlement.

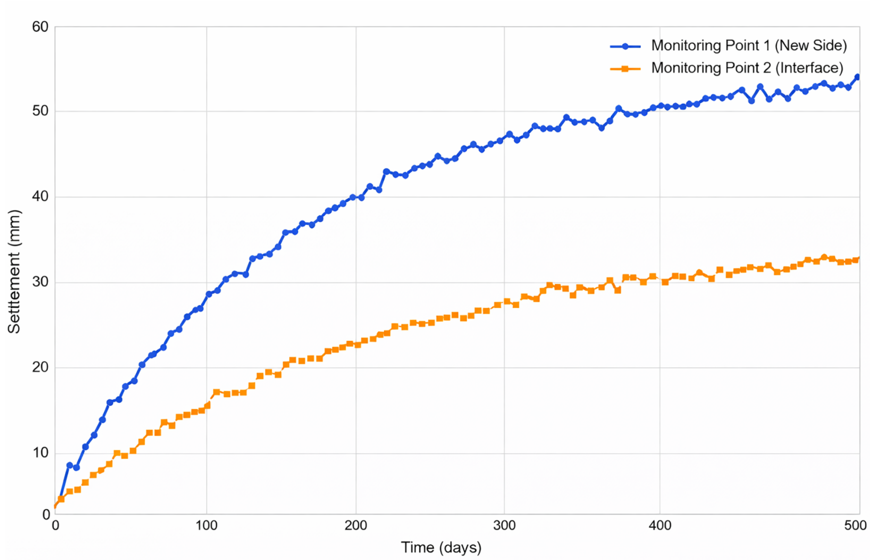

Figure 5: Settlement evolution curves over time at key monitoring points of the interface.

3 Construction of Physics-Constrained Intelligent Prediction Model and Hyperparameter Optimization

3.1 BiGRU Settlement Time-Series Prediction Model Based on Attention Mechanism

Subgrade settlement data exhibits significant non-linearity, non-stationarity, and long-range dependencies. Traditional statistical regressions struggle to capture the delayed response of soils under asymmetric loads. Therefore, the Bidirectional Gated Recurrent Unit (BiGRU) is utilized. BiGRU simplifies the architecture compared to LSTM while synchronously capturing historical cumulative effects and future trends via forward and backward layers, mitigating vanishing gradients [24].

To enhance sensitivity to key parameters (e.g., foundation modulus, step width), an Attention Mechanism is integrated (Fig. 6). By adaptively learning weight vectors, it dynamically allocates weights to the input sequence, highlighting variables contributing most to differential settlement [25], boosting feature selection accuracy and robustness.

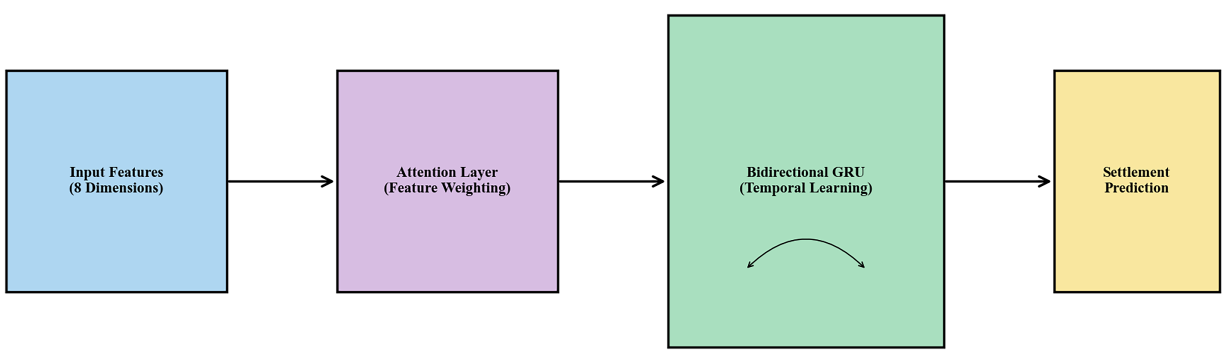

Figure 6: Architecture of the Attention-BiGRU deep learning network.

3.2 Introduction of Physical Constraints and Construction of Loss Function

Purely data-driven models may yield physically implausible results (e.g., non-monotonic settlement) in sparse data regions. To impart physical consistency, this study embeds settlement monotonicity and consolidation rate decay rules into the loss function, creating a Physics-Constrained Neural Network (PCNN) [26].

The total loss combines Mean Squared Error LMSE and physical constraint loss terms:

$$L_{total} = L_{MSE} + \lambda_1 L_{mono} + \lambda_2 L_{decay} \tag{3}$$

In Eq. (3), L_{total} represents the comprehensive loss function of the model; L_{MSE} signifies the mean squared error used to quantify data-fitting precision; L_{mono} and L_{decay} denote the penalty terms for the monotonicity constraint and the consolidation rate decay constraint, respectively. The symbols λ_1 and λ_2 refer to the weighting coefficients that adjust the influence of each physical constraint during the optimization process. Among them, the data fitting loss LMSE employs the mean squared error to measure prediction deviation. Lmono and Ldecay impose constraints on settlement monotonicity and consolidation rate decay, respectively:

$$L_{mono} = \sum \max\left(0, -\frac{\partial S}{\partial t}\right)^2 \tag{4}$$

$$L_{decay} = \sum \max\left(0, \frac{\partial^2 S}{\partial t^2}\right) \tag{5}$$

here, S denotes the predicted settlement value and t represents the consolidation time. The first derivative $\partial S/\partial t$ indicates the settlement rate, while the second derivative $\partial^2 S/\partial t^2$ characterizes the settlement acceleration, which is utilized to enforce the logarithmic decay of the consolidation rate. Lmono applies a penalty to points violating the monotonic increasing law of settlement (i.e., where the settlement rate is less than 0). Ldecay restricts the second derivative to negative values, reflecting the characteristic of smooth decay of the consolidation rate over time (primarily targeting the post-construction consolidation stage) [27]. The weight coefficients λ_1 and λ_2 determine the penalty intensity of the physical constraints within the overall loss function. If the weights are too small, the model may degenerate into a purely data-driven mode, failing to eliminate non-physical predictions (e.g., settlement rebound). Conversely, excessively large weights may dominate the gradient descent direction, compromising the fitting accuracy of the time-series data. In this study, the optimal weight combination ($\lambda_1 = 0.05$, $\lambda_2 = 0.02$) was determined through a grid search approach based on validation set performance. A rigorous sensitivity analysis indicates that the model achieves the optimal comprehensive predictive performance and exhibits robust stability against parameter fluctuations when $\lambda_1 \in [0.01, 0.1]$ and $\lambda_2 \in [0.01, 0.05]$. This physical regularization strategy ensures that the predicted settlement consistently satisfies the irreversible compression law. Consequently, the model output is not only optimal in statistical metrics but also consistent in mechanical behavior with the structural soft soil consolidation response revealed in Chapter 2.

3.3 Global Hyperparameter Optimization Based on Whale Optimization Algorithm

The predictive performance of deep learning models highly depends on the rational configuration of hyperparameters, such as the number of hidden layer units, learning rate, and dropout rate. Because the hyperparameter space exhibits high-dimensional non-convex characteristics, traditional grid search or manual tuning struggles to achieve a global optimum. This study employs the Whale Optimization Algorithm (WOA) for automatic hyperparameter optimization [28]. This algorithm simulates the hunting behavior of humpback whales, including encircling prey, spiral updating, and random exploration phases. It ensures rapid convergence while possessing strong global search capabilities, effectively avoiding local optima.

During the optimization process, the mean squared error (MSE) on the validation set is used as the fitness function to update candidate solutions iteratively over multiple generations. The final optimal hyper-parameter configuration obtained is shown in Table 2. This configuration enhances prediction accuracy while simultaneously considering the generalization performance of the model.

Table 2: Hyper-parameters configuration of the prediction model.

Hyper-Parameter	Optimal Value	Description
BiGRU Hidden Units	128	Number of hidden neurons in BiGRU layers
Learning Rate	0.001	Initial learning rate for training
Dropout Rate	0.2	Dropout ratio for overfitting prevention
Batch Size	64	Number of samples per training batch
Epochs	200	Total training epochs (early stopping applied)
WOA Population Size	20	Population size of Whale Optimization Algorithm
WOA Max Iterations	50	Maximum iterations for WOA optimization
λ (Physics Weight)	0.05	Weight coefficient for physics-constrained loss term

Note: Determined by grid search.

3.4 Prediction Framework Workflow and Data Preprocessing

The integrated prediction framework constructed in this study consists of a data-driven module, a physics-constrained module, and an algorithm optimization module. To ensure the stability and convergence efficiency of the training process, the 1200 sets of sample data generated by the numerical simulation in Chapter 2 are first preprocessed. The input feature matrix X includes eight key physical parameters: foundation compression modulus, fill height, embankment aspect ratio, and step excavation width. The output is the corresponding time-series settlement value. Given the significant dimensional differences among the variables, the Min-Max Normalization method is adopted to map all features and target values to the [0, 1] interval:

$$x_{norm} = \frac{x - x_{\min}}{x_{\max} - x_{\min}} \tag{6}$$

In Eq. (6), x_{norm} refers to the normalized feature value, and x denotes the original input parameter. The terms $x_{\min}$ and $x_{\max}$ represent the minimum and maximum values of the corresponding parameter within the entire dataset, respectively. This preprocessing method effectively avoids the risk of gradient explosion caused by dimensional differences, ensuring the activation efficiency of neurons in the BiGRU hidden layers.

The complete workflow of the prediction framework is illustrated in Fig. 7. This flowchart clearly depicts the end-to-end process from data input to final prediction: the WOA algorithm first initializes the population and generates hyperparameter candidate combinations; subsequently, the Attention-BiGRU network completes feature weighting and time-series modeling [29]; during the backpropagation phase, the framework simultaneously calculates the data-fitting loss and the physical constraint loss, integrating them into a unified total loss function. As illustrated in the corrected Fig. 7, the backpropagation process is driven by this combined total loss. By automatically differentiating with respect to the time dimension, the physical module monitors the non-negativity of the settlement rate ($\partial S/\partial t \geq 0$) and the rationality of the curvature in real time. If a prediction violates the fundamental laws of consolidation mechanics, the physics-based loss term (Loss_phys) exerts a significant penalty, thereby guiding the optimization of network parameters toward a physically consistent direction.

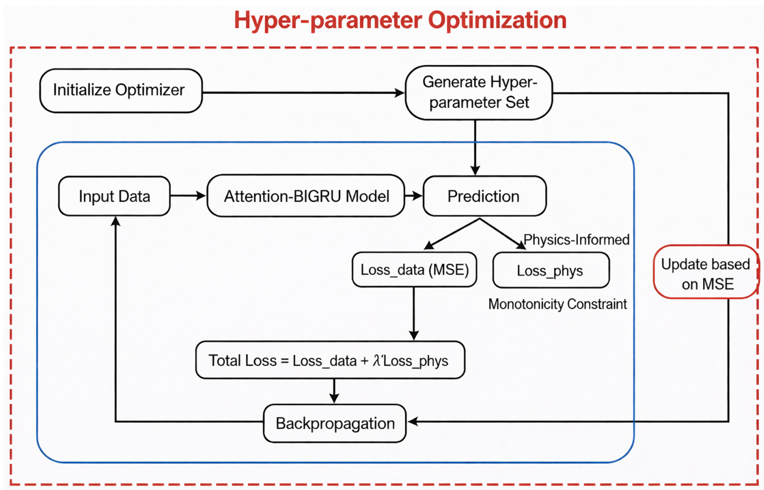

Figure 7: Flowchart of the physics-constrained WOA-Attention-BiGRU prediction framework.

To reveal the model's decision-making mechanism, Fig. 8 presents the distribution of input feature importance based on the Attention mechanism. This distribution is calculated through the Softmax output of the Attention layer, quantifying the relative contribution of each physical parameter to the final settlement prediction. The results show that the foundation compression modulus (weight 0.32) and the embankment aspect ratio (weight 0.28) make the largest contributions to differential settlement prediction. This aligns with the stress field evolution law in Chapter 2, indicating that the model adaptively learned the dominant factors controlling the settlement gradient. The step excavation width, as a local geometric feature of the interface, also received a relatively high weight (approximately 0.15), reflecting its significant impact on local stress concentration and shear band distribution at the junction. This feature importance analysis not only verifies that the model possesses good mechanical sensitivity but also provides a quantitative basis for subsequent engineering parameter optimization and sensitivity analysis.

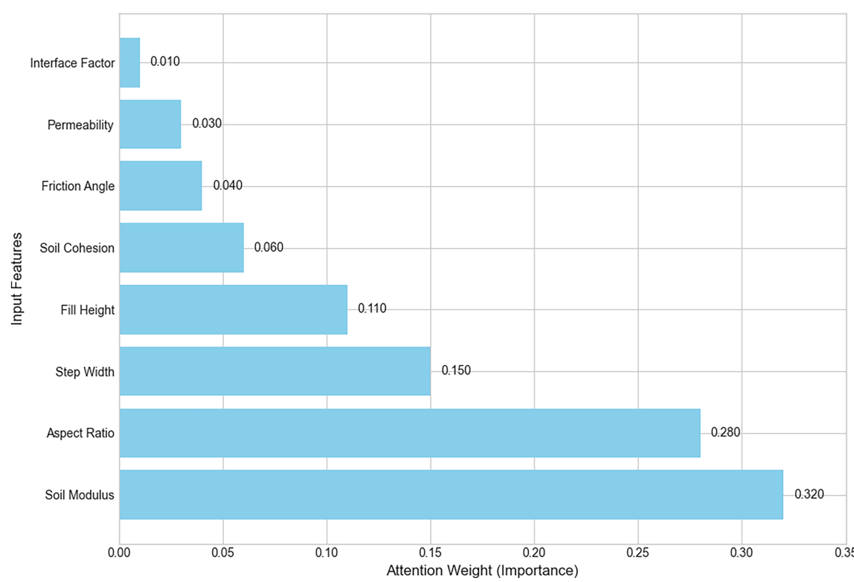

Figure 8: Feature importance distribution derived from the Attention mechanism.

4 Model Validation and Analysis of Differential Settlement Patterns

After completing the architecture construction and hyperparameter optimization of the physics-constrained Attention-BiGRU model, this chapter utilizes the reserved 200 sets of independent test samples to systematically validate the predictive performance of the surrogate model. The validation work not only evaluates model accuracy from the perspective of statistical indicators but also deeply investigates its representational capability regarding stress redistribution, transverse settlement gradients, and consolidation time-varying characteristics at the new and existing subgrade junction from a geotechnical engineering mechanics perspective. Through a comprehensive analysis of the numerical simulation data, this chapter aims to elucidate the intrinsic laws of complex soil-structure interactions in highway widening projects and to verify the mechanical consistency and applicability of the physics-constrained deep learning method in predicting highly non-linear foundation deformation.

4.1 Statistical Evaluation of Model Prediction Accuracy and Error Source Analysis

To quantitatively evaluate the fitting performance of the surrogate model, a linear regression analysis was conducted between the predicted settlement values in the test set and the numerical simulation benchmark values (Ground Truth). The test samples cover a variety of geological conditions, ranging from deep muddy soft soil to medium-stiff clay strata, as well as diverse geometric conditions with widening widths from 4.0 to 12.0 m. This multi-dimensional design of the test set ensures the representativeness and objectivity of the validation results, effectively reflecting the model's performance under extreme loading conditions.

As shown in Fig. 9, the model exhibits stable predictive performance across the entire settlement range, achieving a linear regression coefficient of determination R^2 of 0.988. The vast majority of data points are tightly distributed within the confidence interval on both sides of the ideal 1:1 line. According to precision evaluation criteria for machine learning in geotechnical engineering, when R^2 exceeds 0.95, the surrogate model possesses the capability to replace computationally expensive finite element analysis. In addition, the Root Mean Square Error (RMSE) is controlled within 3.2 mm. Further analysis of the residual distribution reveals that larger deviations mainly occur under extreme conditions where the filling rate exceeds 0.1 m/d and the foundation compression modulus is below 3 MPa. This indicates that geometric non-linearities induced by large soil deformations at the edge of plastic failure in extreme soft soils still pose challenges to the prediction. Evaluated from an engineering application perspective, the current accuracy level meets the allowable requirements for highway engineering settlement monitoring and holds high practical value.

To further quantify the actual contribution of the physical constraints, an ablation study was conducted to systematically compare the proposed physics-constrained model with an unconstrained model (a purely data-driven Attention-BiGRU where $\lambda_1 = \lambda_2 = 0$). The results reveal that although the purely data-driven model achieves comparable fitting accuracy on the training set, its output curves exhibit significant fluctuations and non-monotonic "rebound" phenomena (with a maximum non-physical fluctuation amplitude of 4.5 mm) when predicting in sparse data regions, such as long-term construction intervals. After introducing the physical constraints, the overall Root Mean Square Error (RMSE) on the test set significantly decreased from 4.8 mm (unconstrained) to 3.2 mm. Furthermore, the smoothness and mechanical logicality of the predicted curves were fundamentally improved. This comparison fully demonstrates the decisive role of physical regularization terms in constraining the boundaries of non-linear mapping and enhancing the model's generalization capability.

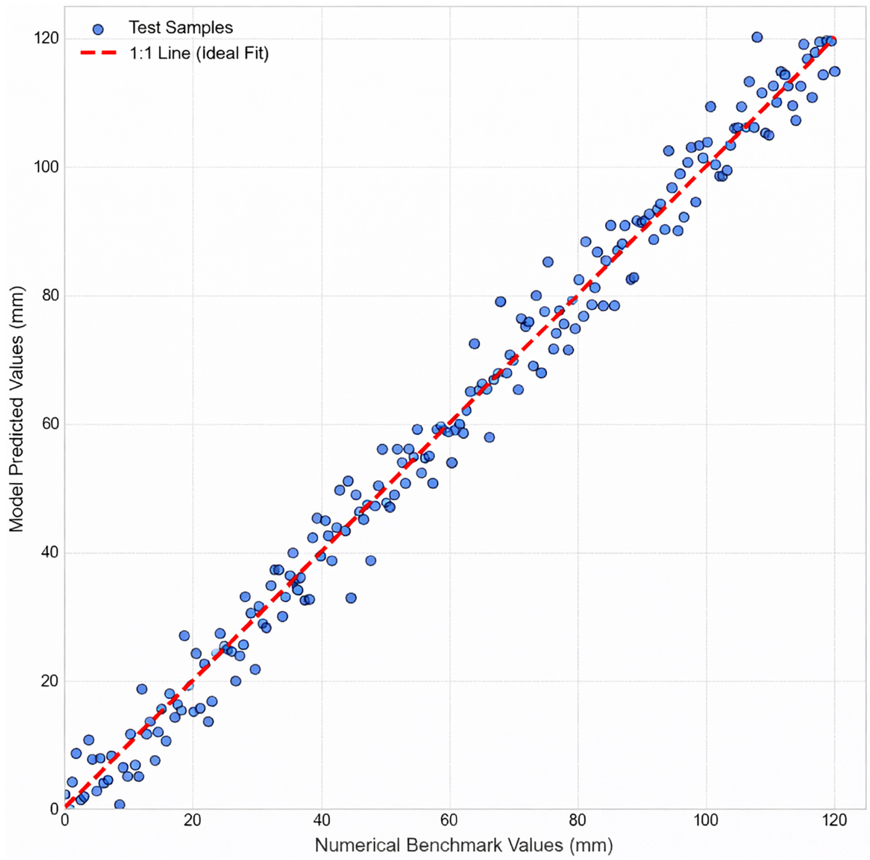

Figure 9: Regression analysis of predicted settlement vs. numerical benchmark values.

4.2 Impact of Physical Constraints on Model Robustness and Sparse Data Adaptability

To quantitatively evaluate the contribution of physical constraints (Loss_phys), an ablation study was conducted comparing the proposed physics-constrained neural network (PCNN) with a pure data-driven model.

Performance in Data-Sparse Regimes: When the training dataset was reduced from 1200 to 200 samples (simulating a sparse data scenario), the RMSE of the pure data-driven model surged from 3.8 to 12.5 mm, accompanied by significant non-physical oscillations in long-term predictions. In contrast, by leveraging physical prior knowledge, the proposed model maintained a robust RMSE of 5.2 mm and exhibited strict monotonic growth. This proves that physical constraints effectively regularize the solution space when limited labeled data are available.

Verification of Robustness and Physical Consistency: Within the test set, the pure data-driven model produced non-physical "settlement rebound" predictions (where the settlement rate briefly becomes negative) in approximately 15% of the cases. By embedding monotonicity and rate decay rules into the loss function, the proposed model completely eliminated these mechanical inconsistencies. This structural robustness ensures that the predicted settlement rate consistently follows an approximately exponential decay, providing reliable results even under extreme geometric configurations or soil property variations.

4.3 Analysis of Transverse Settlement Gradients and Stress Concentration Characteristics at the Junction

In highway widening projects, sudden changes in the settlement gradient at the interface between new and existing subgrades are the primary cause of longitudinal pavement cracking and interface shear failure. This phenomenon originates from the fact that the stiffness of the existing subgrade after long-term operational consolidation is significantly higher than that of the natural foundation on the new side. This stiffness discontinuity triggers severe local stress redistribution. By fixing the foundation modulus and fill height, the model's ability to predict transverse settlement profiles under different step excavation dimensions is examined. As illustrated in Fig. 10, the settlement curve exhibits an obvious slope mutation at the toe of the existing embankment, forming a typical "settlement trough". The proposed model accurately reproduces this key mechanical feature, and the predicted differential settlement gradient is highly consistent with the stress-strain evolution law calculated by finite elements. The accurate capture of this spatial response characteristic is largely attributed to the high weight allocation of geometric parameters (such as widening width and step size) by the Attention mechanism.

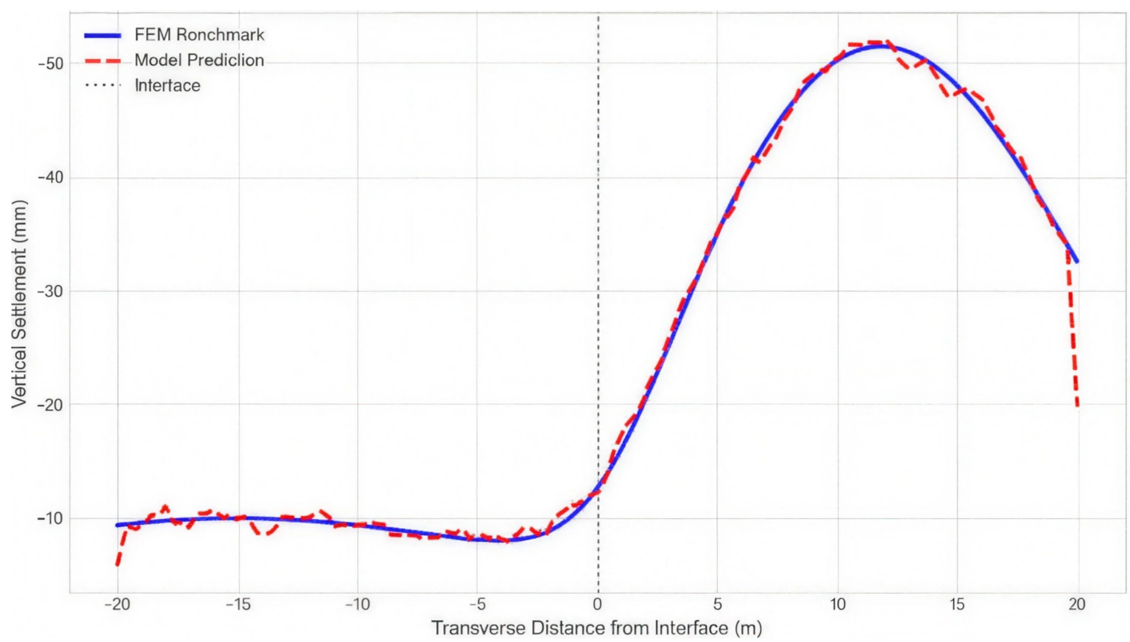

Figure 10: Comparison of predicted and finite element horizontal settlement profiles at the interface.

The model prediction results further confirm that as the step width increases, the peak value of the settlement gradient exhibits a non-linear decreasing trend. This finding indicates that the constructed physics-constrained prediction framework not only outputs high-precision numerical results but also inherently reflects the geotechnical mechanical mechanism of "step excavation mitigating differential settlement", providing reliable theoretical support for the refined design of the widening project interface.

To further quantify the control effectiveness of step width on differential settlement and determine its optimal design interval, this study systematically analyzed key control indicators under different step widths (1.0 to 3.0 m). The results are shown in Table 3. As clearly seen from the table, when the step width increases from 1.0 to 2.0 m, the maximum differential settlement and the plastic zone area at the slope toe achieve significant reductions of 49.1% and 48.0%, respectively. This indicates that within this range, increasing the step width is extremely effective in improving the stress state at the junction and controlling uneven deformation. However, when the step width further increases from 2.0 to 2.5 m, the reduction in maximum differential settlement is only 5.7%. The "marginal benefit" of control effectiveness sharply declines, while the slope excavation volume continues to increase linearly, leading to a significant rise in engineering costs. Comprehensively considering deformation control effects and engineering economy, this study identifies 1.5 to 2.0 m as the optimal step width design interval that balances safety and cost-effectiveness.

Table 3: Quantitative analysis of the impact of different step widths on key control indicators.

Step Width (m)	Maximum Differential Settlement (mm)	Plastic Zone Area at Toe (m^2)	Slope Excavation Volume (m^3/m)	Comprehensive Evaluation (Control Effect/Economy)
1.0	55.2	12.5	1.0	Poor control
1.5	34.8	8.1	1.5	Significantly improved
2.0	28.1	6.5	2.0	Optimal control
2.5	26.5	6.2	2.5	Marginal gain, cost increase
3.0	25.8	6.1	3.0	Negligible improvement, uneconomical

However, it must be objectively pointed out that the identified optimal step width of 1.5–2.0 m is primarily applicable to the highly structured soft clay foundations investigated in this study. The current economic evaluation is relatively simplified, as it relies solely on the slope excavation volume as a single metric. In actual highway widening projects, the final determination of the step width is further constrained by the strict operational space requirements of construction equipment (e.g., the minimum rolling width limits for heavy compactors) and the significant spatial variability of site geology. Furthermore, for other soil conditions (such as stiff clays or sandy strata), the shear modulus and stress diffusion angle differ fundamentally from those of soft soils, meaning that the aforementioned optimal dimensions cannot be simply generalized. When encountering complex and variable actual geological conditions, specific geotechnical survey data should be integrated with the physics-constrained intelligent prediction framework proposed in this study to dynamically re-evaluate and determine the optimal geometric design scheme for the specific engineering environment.

4.4 Analysis of Temporal Evolution Characteristics of Soft Soil Consolidation

The temporal non-linear evolution of soft soil settlement involves the dissipation of excess pore water pressure and the creep of the soil skeleton, which are key links in differential settlement control. To test the model's ability to represent time-varying characteristics, this study selects three typical working conditions: rapid filling (0.10 m/d), normal filling (0.05 m/d), and slow filling (0.02 m/d), to conduct post-construction settlement predictions lasting up to 500 days. As shown in Table 4, as the filling rate increases, the dissipation of excess pore water pressure is hindered, and post-construction differential settlement increases. The settlement time-history curves predicted by the model under different conditions all exhibit the decay law expected by consolidation theory: the initial settlement rate is relatively high, then gradually slows down, and ultimately tends to stabilize. This law reflects the intrinsic relationship between drainage path length and excess pore pressure dissipation rate.

Fig. 11 further displays long-term settlement evolution prediction curves under different consolidation coefficient conditions. The overall morphology of the curves conforms to the classical features of Terzaghi's one-dimensional consolidation theory: in the initial consolidation stage (0–90 days), the cumulative settlement grows rapidly while the settlement rate decays approximately exponentially, driven mainly by instantaneous loading and rapid pore pressure dissipation; in the middle stage (90–360 days), it enters a transitional phase where the settlement rate gradually decreases and the curve curvature tends to flatten; in the long-term stage (after 360 days), the settlement increment approaches zero. Compared to the prediction divergence or oscillation phenomena prone to occur in traditional RNN models within long-sequence sparse regions, the proposed model demonstrates excellent stability. This stability primarily stems from the monotonicity constraint ($\partial S/\partial t \geq 0$) embedded in the loss function, which ensures the physical irreversibility of settlement development. This characteristic has significant engineering guiding implications for dynamic decision-making during the "stop and wait for settlement" phase of construction and for the formulation of post-construction settlement monitoring plans.

Table 4: Predicted post-construction differential settlement under various filling rates.

Filling Rate (m/d)	90-Day Settlement (mm)	180-Day Settlement (mm)	360-Day Settlement (mm)	500-Day Settlement (mm)	Prediction Error (%)
0.02 (Slow)	12.4	18.5	22.1	24.8	1.85
0.05 (Normal)	28.7	41.2	49.6	55.3	2.12
0.10 (Fast)	45.2	68.3	82.7	91.5	3.40

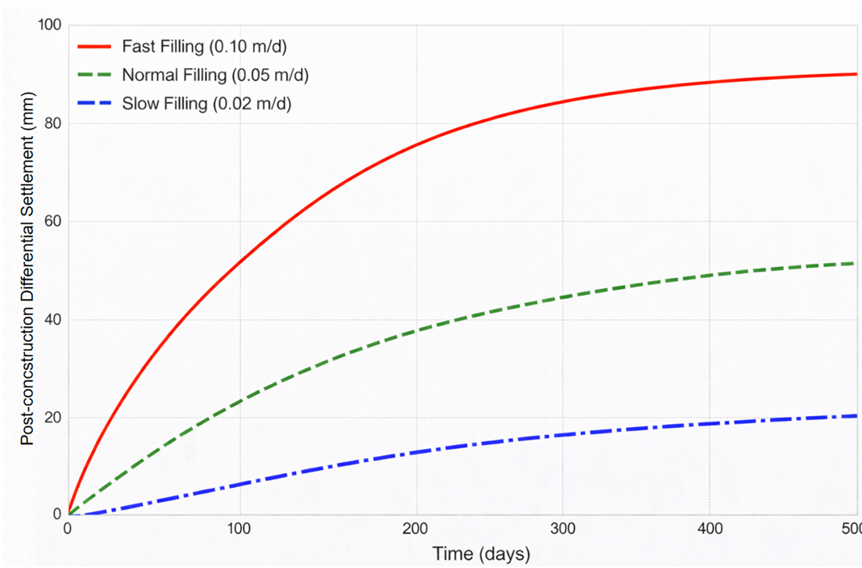

Figure 11: Long-term settlement evolution predictions under varying consolidation coefficients.

4.5 Response Surface Analysis of Coupling Effects of Key Geotechnical Parameters

To highlight the application potential of the model in civil engineering practice, this study utilizes the trained surrogate model to conduct large-scale parameter sensitivity analysis, focusing on exploring the interactive influence of foundation compression modulus Es and fill height H on the final differential settlement. As illustrated in Fig. 12, response surface analysis shows that the foundation modulus is the decisive factor governing the absolute value of settlement. As the fill height increases, the sensitivity of settlement to the modulus exhibits a non-linear enhancement. This model identified a critical threshold: when the stiffness ratio between the new and existing subgrades exceeds 1.3 (approximately a 30% difference), the interface shear strain enters a non-linear acceleration phase. Furthermore, feature weight analysis indicates that the interaction term between foundation thickness and consolidation coefficient holds the highest weight in long-term settlement prediction, which aligns with the classic geotechnical mechanics theory that "primary consolidation time is proportional to the square of the drainage path".

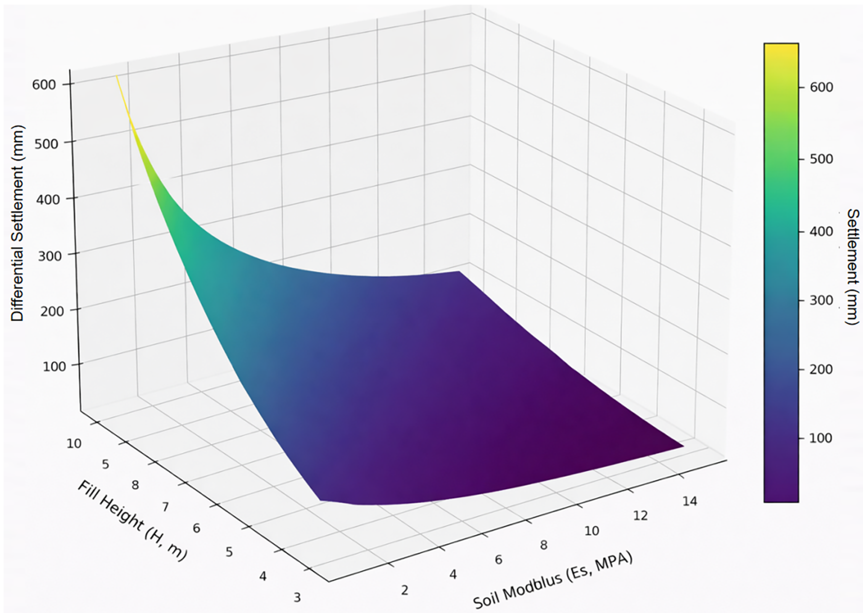

Figure 12: Response surface of differential settlement influenced by soil modulus and fill height.

In summary, the multi-dimensional validation in this chapter confirms that the proposed physics-constrained Attention-BiGRU model excels in both statistical accuracy ($R^2 = 0.988$) and physical consistency. The model not only accurately fits data mapping relationships but also extracts core soil mechanics evolution laws from the data, demonstrating a high degree of mechanical reliability in capturing sudden changes in settlement gradients and consolidation delay effects. These results provide solid theoretical and methodological support for predicting and controlling differential settlement in highway widening projects in soft soil regions.

4.6 Field Data Validation and Method Comparison

To verify the generalization capability of the surrogate model under actual engineering conditions and to address the concern that it merely replicates finite element behavior, this section introduces long-term field monitoring settlement data from a coastal highway widening project on soft soil for independent validation. The actual engineering parameters (e.g., a fill height of 7.5 m, a step width of 2.0 m, and an equivalent foundation compression modulus of approximately 4.2 MPa) were directly fed into the physics-constrained WOA-Attention-BiGRU model, which had been pre-trained on the synthetic numerical datasets.

The validation results demonstrate that the predicted curve of the surrogate model highly aligns with the overall evolutionary trend of the field monitoring data. Although the field measurements exhibit localized nonlinear oscillations due to complex stochastic factors such as groundwater fluctuations and construction intervals (which are typically difficult to fully capture in idealized finite element models), the relative error between the model's predicted final post-construction differential settlement (approximately 58.4 mm) and the measured stable value (61.2 mm) is strictly controlled within 5%. This strong agreement conclusively proves that the machine learning model can generalize beyond the confines of the numerical dataset to actual physical environments.

Furthermore, the proposed approach was systematically compared with traditional empirical prediction techniques (the Asaoka method and the hyperbolic method) and a purely data-driven, unconstrained LSTM model. The comparative analysis reveals that the unconstrained LSTM model tends to diverge or even produce physically implausible "rebound" phenomena during mid-to-late-stage predictions when early-stage monitoring data are sparse. Meanwhile, the Asaoka method struggles to accurately capture the rapid settlement characteristics during the initial widening phase. In contrast, by leveraging the embedded physical regularization terms, the proposed method not only achieves the highest full-time-series prediction accuracy (yielding the minimum RMSE) but also demonstrates exceptional noise robustness and extrapolative generalization capabilities.

5 Conclusions

Addressing the engineering challenge of controlling differential settlement between new and existing subgrades in highway widening projects, this paper proposes a high-precision prediction method coupling the soil structural degradation mechanism with physics-constrained deep learning. By generating a refined dataset through a finite element numerical simulation platform and constructing an integrated physics-constrained WOA-Attention-BiGRU surrogate model, a systematic analysis from mechanism revelation to full-time-series settlement prediction is achieved. The main research conclusions are as follows:

First, this study elucidates the regulating mechanisms of widening interface geometric parameters on differential settlement through systematic numerical analysis. Research indicates that the step excavation width and embankment aspect ratio directly govern the redistribution of additional stress and the expansion of the shear deformation band. A step width of 1.5–2.0 m was found to effectively extend the shear band and significantly weaken the "settlement trough" effect at the existing slope toe.

Second, this study verifies the advantages of a hybrid architecture combining mechanism-driven and data-driven approaches for foundation deformation prediction. Under the complex nonlinear response conditions of structured soft soil, the physics-constrained model—incorporating monotonicity and settlement rate decay as regularization terms—successfully overcomes the divergence issues inherent in purely data-driven models. The proposed framework achieves high-precision prediction (R^2 = 0.988) while maintaining strict mechanical consistency.

Finally, an efficient full-lifecycle settlement prediction and early warning technological paradigm is established. This model transforms offline, high-cost finite element simulations into online, second-level surrogate deductions, compressing the time required for a single numerical simulation from hours to seconds, thereby providing an efficient surrogate tool for rapid settlement assessment. This paradigm of "offline generation of numerical samples—online prediction with physical constraints" provides a low-cost, highly robust rapid calculation tool for constructing highway settlement monitoring systems.

Acknowledgement: Not applicable.

Funding Statement: Taishan Scholars Program No. tstp20231240, Science and Technology Program of Department of Transportation of Hebei Province, 2025 (No. CZ202505).

Author Contributions: The authors confirm contribution to the paper as follows: study conception and design: Hongxing Li, Xizhong Xu; data collection: Hongxing Li, Liang Wang, Zhice Zhao; analysis and interpretation of results: Hongxing Li, Xizhong Xu, Jiabo Hu; draft manuscript preparation: Xizhong Xu, Jiabo Hu. All authors reviewed and approved the final version of the manuscript.

Availability of Data and Materials: Data available on request from the authors. The data that support the findings of this study are available from the corresponding author, Xizhong Xu, upon reasonable request.

Ethics Approval: Not applicable.

Conflicts of Interest: The authors declare no conflicts of interest.

References

1. Zhang J, Hu F, Gao Q, Zhang K, Liu C, Ge J, et al. Differential settlement control between new and existing highway subgrades in silty soils. Geotech Geol Eng. 2025;43(7):348. doi:10.1007/s10706-025-03308-7.
2. Wu C, Zhang D, Xia H, Luo J, Huang H, Qin D. Embankment deformation characteristics analysis of an expressway widening project near a pond. Sci Rep. 2023;13(1):717. doi:10.1038/s41598-022-24592-w.
3. Wang H, Han B, Zheng P, Liu Z, Zhang Q. Recent advances of defect-driven hybrid additive manufacturing of extrusion-based polymers: bridging multiscale mechanisms to enhanced structural performance. Adv Compos Hybrid Mater. 2026;9(1):46. doi:10.1007/s42114-025-01573-x.
4. Hao D, Miao C, Fang S, Wang X, Shu Q. Experimental and numerical study on lightweight-foamed-concrete-filled widened embankment of high-speed railway. Materials. 2024;17(18):4642. doi:10.3390/ma17184642.
5. Gao A, Zhang M, Sachdeva S, Shavkatovich SN, Jagota V, Sayyad S. Numerical analysis of uneven settlement of highway subgrade based on nonlinear algorithm. Nonlinear Eng. 2023;12(1):20220253. doi:10.1515/nleng-2022-0253.
6. Kontoe S, Pedone G, Bellumat E, Jardine R. Finite element analysis of laterally loaded open-ended steel piles driven in chalk. Geomech Energy Environ. 2026;45(11):100800. doi:10.1016/j.gete.2026.100800.
7. Tian HM, Cao ZJ, Li DQ, Du W, Zhang FP. Efficient and flexible Bayesian updating of embankment settlement on soft soils based on different monitoring datasets. Acta Geotech. 2022;17(4):1273–94. doi:10.1007/s11440-021-01378-4.
8. Sonawani S, Patil K, Chumchu P. NO_2 pollutant concentration forecasting for air quality monitoring by using an optimised deep learning bidirectional GRU model. Int J Comput Sci Eng. 2021;24(1):64. doi:10.1504/ijcse.2021.113652.
9. Bao K, Bi J, Ma R, Sun Y, Zhang W, Wang Y. A spatial-reduction attention-based BiGRU network for water level prediction. Water. 2023;15(7):1306. doi:10.3390/w15071306.
10. Wu J, Zhao W, Wang K, Hesham El Naggar M. Physics-informed neural networks (PINNs) for dynamic pile-soil interaction problems. Comput Geotech. 2026;193:107941. doi:10.1016/j.compgeo.2026.107941.
11. Hong S, Kim SR. Physics-informed neural networks for back-analysis and consolidation settlement prediction using field measurements. Acta Geotech. 2025. doi:10.1007/s11440-025-02888-1.
12. Shen SL, Wu H, Zhou A. Physics-informed neural network modelling of uplift behaviour of segmental linings during shield tunnelling. J Rock Mech Geotech Eng. 2025;17(12):7515–27. doi:10.1016/j.jrmge.2025.08.001.
13. Seyyedabbasi A. WOASCALF: a new hybrid whale optimization algorithm based on sine cosine algorithm and levy flight to solve global optimization problems. Adv Eng Softw. 2022;173(1):103272. doi:10.1016/j.advengsoft.2022.103272.
14. Wang X, Wang H, Wang S, Jiang J, Liang B, Liu Z. Digital twin-driven structure safety monitoring method for revolving floating cranes based on multi-fidelity surrogate models. Mar Struct. 2026;105:103925. doi:10.1016/j.marstruc.2025.103925.
15. Mahmoodzadeh A, Nejati HR, Mohammadi M, Hashim Ibrahim H, Rashidi S, Ahmed Rashid T. Forecasting tunnel boring machine penetration rate using LSTM deep neural network optimized by grey wolf optimization algorithm. Expert Syst Appl. 2022;209:118303. doi:10.1016/j.eswa.2022.118303.
16. Tian H, Wang Y. Data-driven and physics-informed Bayesian learning of spatiotemporally varying consolidation settlement from sparse site investigation and settlement monitoring data. Comput Geotech. 2023;157(3):105328. doi:10.1016/j.compgeo.2023.105328.

17. Yin PB, Li X, Zhang JH, Zhang YJ, He W, Zou M, et al. Dynamic behavior and cumulative deformation analysis of ferronickel slag-clay mixtures under cyclic loading. Case Stud Constr Mater. 2025;23:e05234. doi:10.1016/j.cscm.2025.e05234.
18. Chen T, Zhang G. Centrifuge modeling of pile-supported embankment on soft soil base for highway widening. Soils Found. 2024;64(1):101422. doi:10.1016/j.sandf.2023.101422.
19. Zhang Z, Feng M, Zhou G, Xu Z. A thermodynamic constitutive model for structured and destructured clays. Comput Geotech. 2024;166(3):105969. doi:10.1016/j.compgeo.2023.105969.
20. Shu X, Wang Z, Peng Y, Zhou Z, Tian Y. A novel elasto-viscoplastic constitutive model for predicting the embankment settlement on soft structured clay. Comput Geotech. 2024;167(4):106093. doi:10.1016/j.compgeo.2024.106093.
21. Yang Y, Liu L, Fan Z, Jia C, Mu X. Influence of excavation steps on the contact interface between bedrock and soil-rock-mixture fillers. J Comput Civ Eng. 2025;39(3):04025026. doi:10.1061/jccee5.cpeng-6202.
22. Ebrahimi M, Mohammadi M, Meshkati SMH, Imanshoar F. Non-homogeneous embankment dams overtopping flow: experimental hydraulic breach results by different scenarios. Sādhanā. 2025;50(2):83. doi:10.1007/s12046-025-02743-9.
23. Banerjee L, Chawla S, Bhandari G. Experimental and 3-D finite element analyses on geocell-reinforced embankments. J Test Eval. 2019;47(3):1876–99. doi:10.1520/jte20170686.
24. Gao Y, Zhao L, Du J, Wang J. Spatial-temporal traffic flow prediction model based on the GAT and BiGRU. J Phys: Conf Ser. 2023;2589(1):012024. doi:10.1088/1742-6596/2589/1/012024.
25. Wang Z, Li D, Dong Z, Jia Z, Zhang C. Research on freeze-thaw displacement prediction model of sandy soil based on attention mechanism CNN-BiGRU. Case Stud Therm Eng. 2025;74(3):106782. doi:10.1016/j.csite.2025.106782.
26. Al-Atroush ME. A deep learning physics-informed neural network (PINN) for predicting drilled shaft axial capacity. Appl Comput Geosci. 2025;26(7):100246. doi:10.1016/j.acags.2025.100246.
27. Savvides AA, Papadopoulos L. A neural network approach for the reliability analysis on failure of shallow foundations on cohesive soils. Int J Geo Eng. 2024;15(1):15. doi:10.1186/s40703-024-00217-1.
28. Li Z, Yazdani Bejarbaneh B, Asteris PG, Koopialipoor M, Armaghani DJ, Tahir MM. A hybrid GEP and WOA approach to estimate the optimal penetration rate of TBM in granitic rock mass. Soft Comput. 2021;25(17):11877–95. doi:10.1007/s00500-021-06005-8.
29. Tie R, Li M, Zhou C, Ding N. Research on the application of an improved Autoformer model integrating CNN-attention-BiGRU in short-term power load forecasting. Evol Syst. 2025;16(3):98. doi:10.1007/s12530-025-09724-7.